For a convex crystal region formulae (45,46,47) are simplified since $g(x)\equiv 0$.

APPENDIX II

The coefficients $a_l^{(n)}$ from (39) are:

$$a_0^{(2)}=\tfrac{1}{2} \quad a_1^{(2)}=0 \quad a_2^{(2)}=-\tfrac{1}{3}.$$

For $n\geq 3$

$$a_0^{(n)}=\frac{1}{n!(n-1)!} \quad a_1^{(n)}=\frac{n-2}{n!(n-1)!};$$

$$a_l^{(n)}=\frac{1}{(n+l-1)!}\sum_{k=1}^{l}(-1)^{k-1}\frac{(n+l-k-1)!}{k!}a_{l-k}^{(n-k)} \quad (\text{for } 2\leq l\leq n-2);$$

$$a_{n-1}^{(n)}=\frac{1}{(2n-2)!}\times\left[(-1)^{n-2}+\sum_{k=1}^{n-2}(-1)^{k-1}\frac{(2n-2-k)!}{k!}a_{n-k-1}^{(n-k)}\right];$$

$$a_n^{(n)}=\frac{1}{(2n-1)!}\times\left[n(-1)^{n-1}+\sum_{k=1}^{n-2}(-1)^{k-1}\frac{(2n-k-1)!}{k!}a_{n-k}^{(n-k)}\right].$$

References

COOPER, M. J. & ROUSE, K. D. (1970). *Acta Cryst.* A**26**, 214–223.

HAMILTON, W. C. (1957). *Acta Cryst.* **10**, 629.

MORSE, P. M. & FESHBACH, H. (1963). *Methods of Theoretical Physics*, Part I. pp. 676–692. New York: McGraw-Hill.

VINEYARD, G. H. (1954). *Phys. Rev.* **96**, 93–98.

WERNER, S. A. (1969). *Acta Cryst.* A**25**, 639.

WERNER, S. A. & ARROTT, A. (1965). *Phys. Rev.* (2*A*), **140**, 675–686.

WERNER, S. A., ARROTT, A., KING, S. J. & KENDRICK, H. (1966). *J. Appl. Phys.* **37**, 2343–2350.

ZACHARIASEN, W. H. (1945). *Theory of X-ray Diffraction in Crystals*. New York: John Wiley.

ZACHARIASEN, W. H. (1967). *Acta Cryst.* **23**, 558–564.

Acta Cryst. (1976). A**32**, 641

The Influence of Specimen Geometry on the Determination of X-ray Absorption Correction Factors for Spheres and Cylinders

BY P. A. TEMPEST

Central Electricity Generating Board, Berkeley Nuclear Laboratories, Berkeley, Gloucestershire, England

(*Received* 12 *January* 1976; *accepted* 24 *February* 1976)

A simple numerical method of determining the absorption correction factors for spherical and cylindrical specimens is described. The construction of line profiles of the diffraction peaks for both types of specimen illustrates the origin of errors inherent in all numerical methods of this kind. The difference in line profiles, particularly the line shift, for spherical and cylindrical specimens could influence the choice of specimen geometry for accurate lattice parameter determinations.

1. Introduction

Recent numerical methods of calculating absorption correction factors for spheres and cylinders (Weber, 1967, 1969; Dwiggins, 1974, 1975) have revealed substantial discrepancies with *International Tables for X-ray Crystallography* (1959) of up to 2·5%. The largest errors are associated with low Bragg angles and large values of the product of the linear absorption coefficient and the radius of the specimen, μR, when the diffracted beam emerges from the 'skin' of the specimen only. It appears that these errors are due to inaccurate numerical integration in this region of the specimen. This paper describes the contribution of different regions of spherical and cylindrical specimens to the resultant line profile of the diffraction peaks in an attempt to establish the origin of these errors.

Several analytical and numerical methods (Claasen, 1930; Evans & Ekstein, 1952; Weber 1969; Dwiggins, 1975), whilst yielding the absorption factor do not afford a simple determination of the line profile. Taylor & Sinclair (1945) introduced a strip method for deriving the absorption factor for a cylinder in which the specimen was divided into strips parallel to the direction of the diffracted X-ray beam. From this construction line profiles for cylindrical specimens were determined. In this paper the strip method of Taylor & Sinclair is applied to both spherical and cylindrical specimens and automatic computing methods are used to eliminate time-consuming graphical integration.

2. Calculation of the absorption correction factor

For a non-absorbing medium the intensity of a diffracted X-ray beam is directly proportional to the

irradiated volume, V, of the specimen. If absorption takes place in the specimen then the intensity of the diffracted beam is reduced by a factor

$$A=\frac{1}{V}\iiint \exp\left[-\mu(p+q)\right]dV \qquad (2.1)$$

(*International Tables for X-ray Crystallography*, 1959) where A is the transmission factor, p and q are the path lengths of incident and diffracted X-ray beams respectively, μ is the linear absorption coefficient for the specimen and the integral is taken over the irradiated volume of the specimen. The case for a sphere will be considered first.

Fig. 1 shows the passage of an X-ray beam through any cross section of the sphere. The beam is Bragg reflected through an angle 2θ by any point P at a distance x along a chord AB. The chord is defined by the angle α' which it subtends at the centre of the circle, radius r. A small volume element dV at P can be expressed as

$$dV=dSdx \qquad (2.2)$$

where dS is a small area element whose plane is normal to the diffracted beam and dx is parallel to the plane normal. Thus equation (2.1) can be rewritten as

$$A=\frac{1}{V}\iint\int_0^c \exp\left[-\mu(p+c-x)\right]dxdS \qquad (2.3)$$

where $c=AB=2r\sin\alpha'/2$. For each area element dS we have to calculate the integrand,

$$I=\int_0^c \exp\left[-\mu(p+c-x)\right]dx\,. \qquad (2.4)$$

If p can be expressed as a function of x such that

$$f(x)=\exp\left\{-\mu[F(x)+c-x]\right\} \qquad (2.5)$$

we obtain

$$I=\int_0^c f(x)dx\,, \qquad (2.6)$$

which can be evaluated by Simpson's rule. Although a simple explicit expression for p in terms of $x, F(x)$, cannot be found the problem can be overcome by using the Newton–Raphson numerical method.

If we can find the function

$$g(p)=0 \text{ for all } x \qquad (2.7)$$

and if $g'(p)$ can be easily evaluated numerically, then the real roots of $g(p)$ can be determined in the following way. Suppose p_0 is an approximate value of one of the roots, then an improved value of the root is given by

$$p=p_0+\Delta p \text{ where } \Delta p=-g(p_0)/g'(p_0)\,. \qquad (2.8)$$

$g(p)$ can be determined by solving the three simultaneous equations generated by applying the cosine rule to triangles AIB, AIP and PIB in Fig. 1. We obtain

$$G(x,p)=0 \qquad (2.9)$$

where

$$G(x,p)=2p^2+2x^2-2cx+2cp\cos 2\theta-4xp\cos 2\theta +2\{p^2+x^2-2xp\cos 2\theta\}^{1/2} \times\{p^2+(c-x)^2+2p(c-x)\cos 2\theta\}^{1/2}\cos\frac{\alpha'}{2}\,. \qquad (2.10)$$

If x_i is any value of x in the range $0\le x_i\le c$, then

$$g(p)=G(x_i,p) \qquad (2.11)$$

and

$$g'(p)=G'(x_i,p)\,. \qquad (2.12)$$

Substitution of values of p, obtained from an iterative process using equation (2.8), and x into equation (2.4) eliminates the problem of finding an analytical form of $F(x)$ and enables equation (2.4) to be evaluated by Simpson's rule.

Ideally the spherical specimen is divided into strips of infinitesimal cross-sectional area parallel to the diffracted beam. In practice evaluation of equation (2.4) for all strips of cross-sectional area dS yields a complete solution of equation (2.3). The total contribution to A of each strip is given by

$$A'=\frac{dS}{V_s}\int_0^c \exp\left[-\mu(p+c-x)\right]dx \qquad (2.13)$$

where V_s is the volume of the strip.

This construction of a sphere in which the strips form cylinders of different radii whose coincident axes are parallel to the plane formed by the incident and diffracted beams is shown in Fig. 2(*a*). In contrast Fig. 2(*b*) shows the construction used by other workers in which the axes of the cylinders are normal to the plane formed by the incident and diffracted beams. Each cylinder in Fig. 2(*a*) is easily defined in terms of

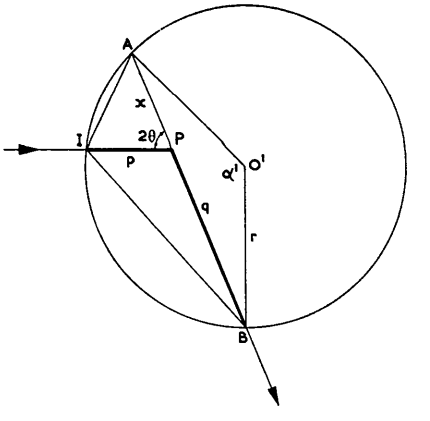

Fig. 1. Passage of X-ray beam through a section of radius r of the sphere.

the angle α which its diameter subtends at the centre of the sphere. The relationships between α, the strip dimensions, and the geometrical quantities of Fig. 1 are illustrated in Fig. 3.

It is readily deduced that

$$c=AB=2R\sin\alpha/2\sin\beta/2 \tag{2.14}$$

and

$$\cos\alpha'/2=\cos\alpha/2\{1-\sin^2\alpha/2\cos^2\beta/2\}^{-1/2}. \tag{2.15}$$

The cross-sectional area of a strip is now given by

$$dS=dydz \tag{2.16}$$

where

$$dy=R\sin\alpha/2\,.\,d\alpha/2 \tag{2.17}$$

and

$$dz=R\sin\alpha/2\sin\beta/2\,.\,d\beta/2\,. \tag{2.18}$$

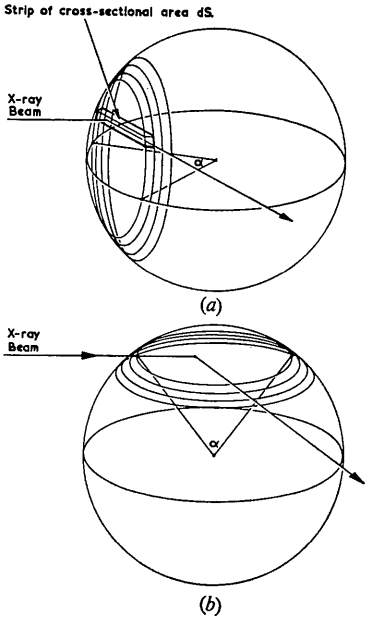

Fig. 2. Construction of spheres (*a*) This paper, (*b*) Other workers.

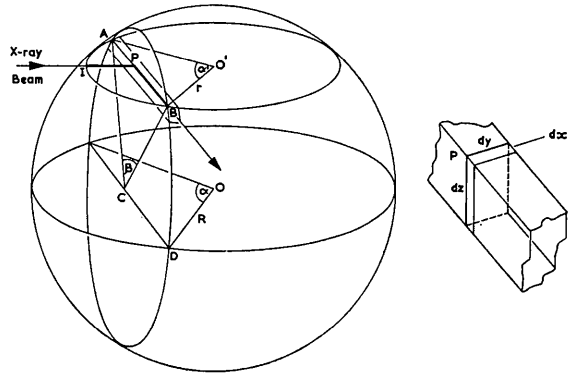

Fig. 3. Diagram to illustrate the geometrical relationship between the circle of Fig. 1 and a spherical specimen.

It may be recalled that by far the largest error in this kind of analysis occurs at high values of μR when the diffracted beam emerges from the outer skin of the specimen only. For greater accuracy in calculating A it is necessary to divide the specimen so that there are many more strips in the skin rather than in the bulk of the specimen. One advantage of the method used in this work can be seen in the form of equations (2.16), (2.17) and (2.18) which show dS to be proportional to $\sin^2\alpha/2\sin\beta/2$. Strips which form the skin of the specimen are identified with small angles of α and/or β so that these strips have smaller cross-sectional areas than those which occur in the bulk of the specimen, and so occur in greater numbers.

Equation (2.3) now reduces to its simplest form

$$A=\frac{R^2}{4V}\int_0^{2\pi}\sin^2\alpha/2\int_0^{2\pi}\sin\beta/2 \times\int_0^{c}\exp\left[-\mu(p+c-x)\right]dx\,d\beta\,d\alpha\,. \tag{2.19}$$

Thus, for a sphere, replacing the integrals over α and β by summations, we obtain

$$A_{\text{sph}}=\frac{3}{16\pi R}\sum_0^{2\pi}\sin^2\alpha/2\,\Delta\alpha\sum_0^{2\pi}\sin\beta/2\,\Delta\beta \times\int_0^{c}\exp\left[-\mu(p+c-x)\right]dx\,. \tag{2.20}$$

For a cylinder the height of each strip, dh, is given by

$$dh=dz=R\sin\alpha/2\sin\beta/2\,d\beta/2\,, \tag{2.21}$$

so that equation (2.19) reduces to

$$A=\frac{R}{2V}\int_0^{h}dh\int_0^{2\pi}\sin\alpha/2\int_0^{c}\exp\left[-\mu(p+c-x)\right]dx\,d\alpha \tag{2.22}$$

and thus,

$$A_{\text{cyl}}=\frac{1}{2\pi R}\sum_0^{2\pi}\sin\alpha/2\Delta\alpha\int_0^{c}\exp\left[-\mu(p+c-x)\right]dx\,. \tag{2.23}$$

A double-precision computer program was written in Fortran IV for evaluating equations (2.20) and (2.23) with increments in x equal to $c/200$ and values of $\Delta\alpha$ and $\Delta\beta$ ranging between $\pi/10$ and $\pi/50$.

3. Discussion of results

In practice it is more convenient to replace the transmission factor A by its reciprocal, the absorption factor A^*. In this way Tables 1 and 2 have been prepared with A^* values for spheres and cylinders calculated over the range μR, $0{\cdot}5\rightarrow 10$ and θ, $0\rightarrow 90°$.

Tables 1 and 2 also include the results of Bond (1959), Weber (1967, 1969) and Dwiggins (1974, 1975).

Table 1. *Values of A* for spheres*

1. This paper (interval in $\alpha=\pi/10$; interval in $\beta=\pi/20$). 2. Dwiggins (1975). 3. Weber (1969). 4. *International Tables for X-ray Crystallography* (1959) reproduced from Bond (1959).

μR	θ = 0°				15				30				45				60				75				90			
	1	2	3	4	1	2	3	4	1	2	3	4	1	2	3	4	1	2	3	4	1	2	3	4	1	2	3	4
0.5	2.076	2.076	2.076	2.076	2.065	2.065	2.065	2.065	2.040	2.040	2.040	2.040	1.990	1.990	1.990	1.990	1.945	1.945	1.945	1.945	1.910	1.910	1.910	1.910	1.897	1.897	1.897	1.897
1.0	4.124	4.124	4.124	4.124	4.031	4.030	4.031	4.030	3.792	3.792	3.792	3.792	3.505	3.505	3.505	3.505	3.250	3.250	3.250	3.249	3.073	3.074	3.073	3.073	3.008	3.009	3.008	3.008
2.0	14.00	14.00	14.00	14.00	12.60	12.59	12.60	12.59	10.03	10.03	10.03	10.03	7.962	7.961	7.961	7.961	6.587	6.587	6.587	6.586	5.785	5.784	5.785	5.784	5.505	5.504	5.505	5.504
3.0	38.38	-	38.38	38.37	29.86	-	29.86	29.85	19.52	-	19.52	19.51	13.62	-	13.62	13.62	10.41	-	10.41	10.41	8.699		8.699	8.697	8.113	-	8.113	8.112
4.0	86.53	-	86.52	86.51	56.04	-	56.03	56.02	30.99	-	30.99	30.98	19.85	-	19.85	19.86	14.43	-	14.43	14.43	11.69		11.69	11.69	10.75	-	10.75	10.75
5.0	167.2	-	167.1	167.1	89.17	-	89.15	89.13	43.55	-	43.55	43.54	26.37	-	26.36	26.35	18.55	-	18.55	18.54	14.72		14.72	14.71	13.40	-	13.40	13.40
6.0	288.1	-	288.2	288.2	127.3	-	127.2	127.1	56.75	-	56.76	56.75	33.04	-	33.03	33.01	22.73	-	22.73	22.71	17.77		17.77	17.76	16.06	-	16.06	16.06
7.0	457.0	-	457.4	457.4	169.0	-	168.9	168.8	70.38	-	70.41	70.42	39.81	-	39.80	39.79	26.93	-	26.93	26.92	20.83		20.83	20.83	18.71	-	18.71	18.72
8.0	681.2	-	682.7	682.6	213.4	-	213.4	213.2	84.30	-	84.35	84.39	46.65	-	46.64	46.62	31.16	-	31.16	31.14	23.91		23.91	23.90	21.37	-	21.38	21.38
9.0	967.9	-	972.0	971.8	260.0	-	259.9	259.7	98.43	-	98.51	98.62	53.53	-	53.52	53.50	35.40	-	35.41	35.39	26.95		26.99	26.98	24.04	-	24.04	24.04
10.0	1324	-	1333	1334	308.3	-	308.2	307.8	112.7	-	112.8	112.9	60.44	-	60.44	60.46	39.65	-	39.66	39.62	30.07		30.07	30.07	26.70	-	26.70	26.70

Table 2. *Values of A* for cylinders*

1. This paper (interval in $\alpha=\pi/10$ for $\mu R\leq 5$ and $\pi/20$ for $\mu R>5$). 2. Dwiggins (1974). 3. Weber (1967). 4. *International Tables for X-ray Crystallography* (1959) reproduced from Bond (1959).

μR	θ = 0				15				30				45				60				75				90			
	1	2	3	4	1	2	3	4	1	2	3	4	1	2	3	4	1	2	3	4	1	2	3	4	1	2	3	4
0.5	2.300	2.300	2.300	2.29	2.284	2.284		2.28	2.240	2.240	2.240	2.24	2.178	2.178	2.178	2.18	2.115	2.115	2.115	2.12	2.068	2.068	2.068	2.07	2.050	2.050	2.050	2.05
1.0	5.091	5.091	5.091	5.06	4.932	4.932	4.933	4.92	4.544	4.544	4.544	4.54	4.102	4.102	4.102	4.10	3.729	3.729	3.729	3.73	3.479	3.479	3.479	3.48	3.389	3.389	3.389	3.39
2.0	21.43	21.43	21.44	21.3	18.24	18.24	18.25	18.2	13.31	13.31	13.31	13.3	9.922	9.921	9.922	9.91	7.895	7.895	7.895	7.91	6.773	6.773	6.774	6.78	6.388	6.389	6.389	6.40
3.0	69.96	-	70.12	69.5	46.85	-	46.86	46.6	26.42	-	26.43	26.4	17.14	-	17.14	17.1	12.58	-	12.59	12.6	10.27	-	10.28	10.3	9.491	-	9.492	9.53
4.0	175.7	-	177.0	175	88.10	-	88.17	87.6	41.45	-	41.48	41.5	24.85	-	24.86	24.9	17.45	-	17.45	17.6	13.84	-	13.85	13.9	12.62	-	12.62	12.7
5.0	357.1	-	363.0	359	136.2	-	136.4	135	57.26	-	57.34	57.5	32.77	-	32.79	32.9	22.38	-	22.39	22.6	17.44	-	17.45	17.6	15.74	-	15.75	15.9
6.0	634.5	-	645.2	636	188.5	-	188.5	187	73.62	-	73.67	74.0	40.81	-	40.83	41.1	27.37	-	27.37	27.7	21.07	-	21.07	21.3	18.87	-	18.88	19.2
7.0	1036	-	1041	1022	243.5	-	243.5	242	90.24	-	90.32	91.1	48.90	-	48.89	49.4	32.37	-	32.38	33.0	24.69	-	24.69	25.1	22.02	-	22.02	22.5
8.0	1555	-	1568	1530	300.7	-	300.6	299	107.1	-	107.2	109	57.05	-	57.10	58.0	37.38	-	37.40	38.3	28.33	-	28.33	29.0	25.15	-	25.16	25.8
9.0	2217	-	2245	2200	359.6	-	359.5	357	124.1	-	124.3	126	65.21	-	65.29	65.6	42.39	-	42.42	43.2	31.97	-	31.97	32.5	28.29	-	28.30	28.9
10.0	3039	-	3092	3050	420.0	-	419.9	417	141.2	-	141.5	143	73.40	-	73.51	74.2	47.42	-	47.46	48.2	35.61	-	35.61	36.1	31.43	-	31.44	31.9

It is generally accepted that the most accurate values published in the literature, especially for high μR values, are those of Weber who, in calculating A_{sph}, used intervals in α of $\pi/200$ in a construction similar to the one shown in Fig. 2(*b*). For $\Delta\alpha$ and $\Delta\beta$ intervals of only $\pi/10$ and $\pi/20$ respectively all newly calculated values of A^*_{sph} and A^*_{cyl} for $\mu R \leq 2{\cdot}0$ are within 0·01% of previous workers' calculations. For A^*_{sph} values with $\theta > 15°$ the largest deviation with the results of Weber is still only 0·08% even for μR values of 10. However, at very low values of θ the deviations from Weber's results increase markedly to a value of 0·7% at $\mu R = 10$ and $\theta = 0$. Although this result reveals the shortcomings of inaccurate numerical integration, a reduction in $\Delta\alpha$ to $\pi/25$ and $\Delta\beta$ to $\pi/50$ immediately reduces this discrepancy to $< 0{\cdot}07\%$. A closer inspection of the results for A^*_{cyl} values shows even greater discrepancies with Weber's results. Even with $\Delta\alpha$ reduced to $\pi/20$ the deviation of A^*_{cyl} at $\mu R = 10$ and $\theta = 0$ has risen to 1·7%. A reduction in $\Delta\alpha$ to $\pi/50$ is required to reduce the deviation to $< 0{\cdot}07\%$.

The different errors in A^*_{sph} and A^*_{cyl} for the same interval in α can be attributed to the different contribution of the skins of the specimens to the overall intensity of the diffracted beam. The origin of these different errors is best illustrated by an investigation of the line profiles for both spheres and cylinders.

4. A comparison of line profiles from spherical and cylindrical specimens

The desire of other workers to use A^*_{cyl} values to calculate A^*_{sph} values, so reducing the number of numerical integrations involved, prevented them from determining the line profiles. In such instances the geometrical construction shown in Fig. 2(*b*) was used, which contrasts with the construction of Fig. 2(*a*) used in the work described here. The line profile for a spherical specimen is made up by considering the contribution of each cylinder in the construction to the overall intensity. Each individual contribution produces a line element whose height is clearly proportional to

$$\sin\alpha/2 \int_0^{2\pi} \sin\beta/2 \int_0^c \exp\left[-\mu(p+c-x)\right]dx\,d\beta$$

where α defines the size and position of each cylinder. Since the cylindrical cross sections which are used to construct a sphere are reduced to rectangles for the construction of a cylinder (see Fig. 4) the profile for a cylinder is made up of line elements whose height is proportional to

$$\int_0^c \exp\left[-\mu(p+c-x)\right]dx$$

and independent of the height of the cylinder. (The derivation of these proportionalities is given in the Appendix).

Figs. 5 and 6 show the variation of basic line shapes with θ for a spherical and cylindrical specimen for μR values of 1·0 and 5·0. For $\mu R = 1{\cdot}0$ the profiles for the sphere are remarkably similar whereas the profiles for the cylinder change significantly at low values of θ. The peak becomes much narrower and shifted from the centre until at $\theta = 0°$ it splits into two narrow peaks.

This splitting of the peak at $\theta = 0°$ is not evident in the case of the sphere for $\mu R = 1{\cdot}0$. For $\mu R = 5{\cdot}0$, however, the diffraction peak at $\theta = 0°$ for the sphere also shows a distinct minimum. Furthermore, the peaks at other values of θ are also much narrower than those associated with a μR value of 1·0. Nevertheless, the most remarkable feature of these profiles at $\mu R = 5{\cdot}0$ is the severe narrowing of the peak for the cylinder at values of θ less than 45°. It is now clear that the total intensity of the peaks below θ values of approximately 15° is produced by diffraction in the skin of the cylinder. Consequently, whilst intervals of α of $\pi/10$ are adequate to derive accurate values of A^*_{sph}, such intervals lead to substantial errors in values of A^*_{cyl}.

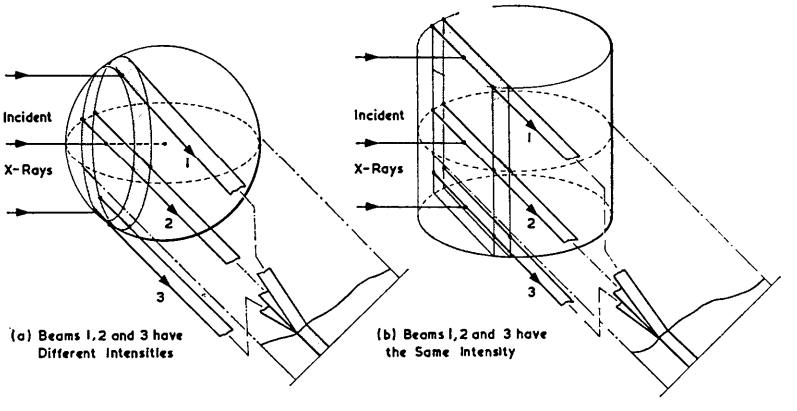

Fig. 4. Construction of line profiles from (*a*) sphere, (*b*) cylinder.

5. Errors in A^*_{sph} and A^{*m}_{cyl} values

It will be assumed that values of A^* are absolutely correct when intervals in α of $\pi/50$ are used. (The error is certainly less than 0·07% when compared to Weber's values at $\mu R = 10{\cdot}0$ and $\theta = 0$.)

If A^*_0 is the correct value then we can define the error in calculated values of A^* as

$$\Delta A^* = \left(\frac{A^*_0 - A^*}{A^*_0}\right) \times 100\% .$$

ΔA^* has been evaluated for both spheres and cylinders under high and low absorption conditions using intervals in α of $\pi/10$.

Fig. 7 shows ΔA^*_{sph} plotted as a function of θ for μR values of 1·0 and 5·0. It is clear that an interval in α of $\pi/10$ is sufficient to keep errors below 0·03% for all values of θ. This result agrees well with the relatively broad line profiles of Fig. 5(*a*) and 6(*a*) for the sphere, which show that even at low values of θ all regions of the sphere contribute significantly to the overall intensity of the peak. Fig. 8 shows ΔA^*_{cyl} plotted as a function of θ for $\mu R = 1{\cdot}0$ and 5·0. Again intervals in θ of $\pi/10$ are sufficient to keep the errors below 0·01% for all θ values at the low absorption value of μR of 1·0. However, when $\mu R = 5{\cdot}0$ large errors in A^*_{cyl} are seen to occur, especially in the region $\theta < 30°$, reaching the relatively very high value of 1·7% at $\theta = 0°$. This difference in ΔA^*_{sph} and ΔA^*_{cyl} shows the unsuitability of A^*_{cyl} values for the calculation of A^*_{sph}, particularly under high absorption conditions and low Bragg angles.

6. Implications of results

It has been shown that specimen absorption produces different line profiles for spheres and cylinders. The origin of the errors occurring in the calculation of absorption correction factors by numerical methods is clearly shown. However, another aspect of specimen absorption which concerns crystallographers is the shift in the diffraction peak of the point of maximum intensity. The displacement of the point of maximum intensity from the centre, ΔR, can be conveniently expressed as a fraction of the sample radius, R. Fig. 9 shows $\Delta R/R$ plotted as a function of θ for both spherical and cylindrical specimens. Between 60° and 90° $\Delta R/R$ falls rapidly to zero for the sphere, whilst it has a value near 1·0 for the cylinder. This angular region is of particular importance in accurate lattice-parameter determinations and, naturally, low values of $\Delta R/R$ are preferred.

It could be inferred from these remarkable variations of $\Delta R/R$ that a spherical specimen is eminently more suitable for lattice-parameter determinations, especially under conditions of high absorption. However, it must be remembered that in the derivation of the line profiles the idealized arrangement of an incident parallel beam of X-rays of uniform intensity was assumed. In practice these conditions rarely occur, the focus of an X-ray tube producing, in general, a slightly diverging X-ray beam of non-uniform intensity.

An assessment of the implication of these results on the commonly used Nelson–Riley plot in accurate lattice-parameter determinations cannot be made at this stage because the correction function,

$$\tfrac{1}{2}\left(\frac{\cos^2\theta}{\theta} + \frac{\cos^2\theta}{\sin\theta}\right)$$

of Nelson & Riley is based theoretically upon the assumption of an incident X-ray beam of non-uniform

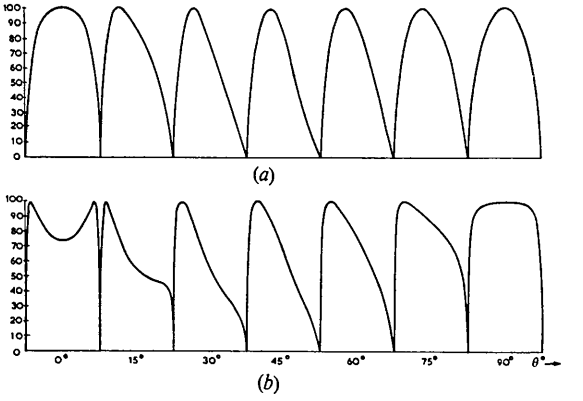

Fig. 5. Line profiles for $\mu R = 1{\cdot}0$. (*a*) Sphere. (*b*) Cylinder.

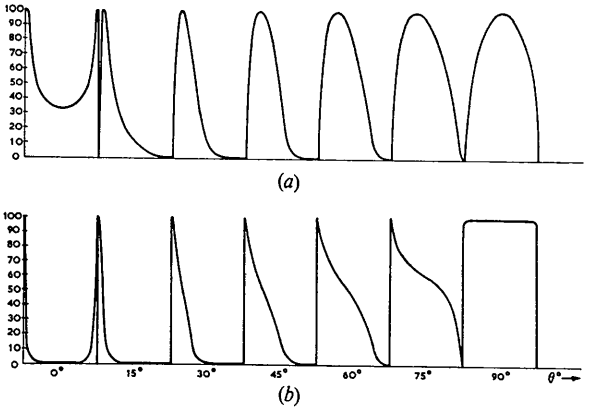

Fig. 6. Line profiles for $\mu R = 5{\cdot}0$. (*a*) Sphere. (*b*) Cylinder.

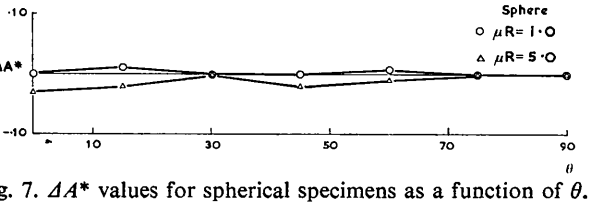

Fig. 7. ΔA^* values for spherical specimens as a function of θ.

intensity emerging from an exponential focus. Nevertheless, for both spherical and cylindrical specimens, the shift of the peak increases with μR emphasizing the need to prepare specimens of small diameter where highly absorbing materials are being used in Debye–Scherrer X-ray powder photography.

Although the consideration of an incident parallel beam of X-rays of uniform intensity demonstrates the necessity to correct measurements for absorption in the specimen, in practice the magnitude of the correction remains a function of the intensity and the nature of the X-ray source also. The effects of non-uniform and non-parallel beams of X-rays on the line profiles of spheres and cylinders will be discussed in a later communication.

This paper is published by permission of the Central Electricity Generating Board.

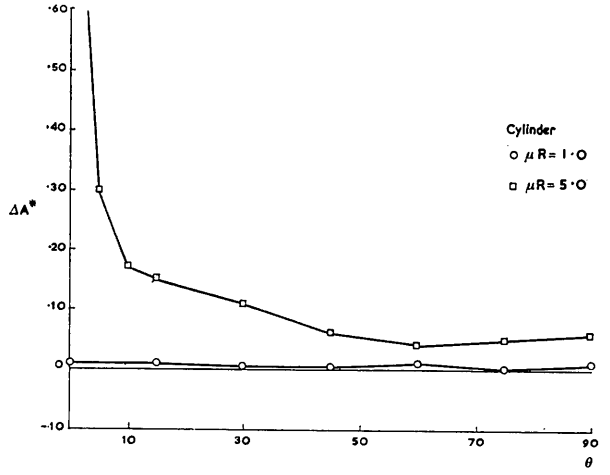

Fig. 8. ΔA^* values for cylindrical specimens as a function of θ.

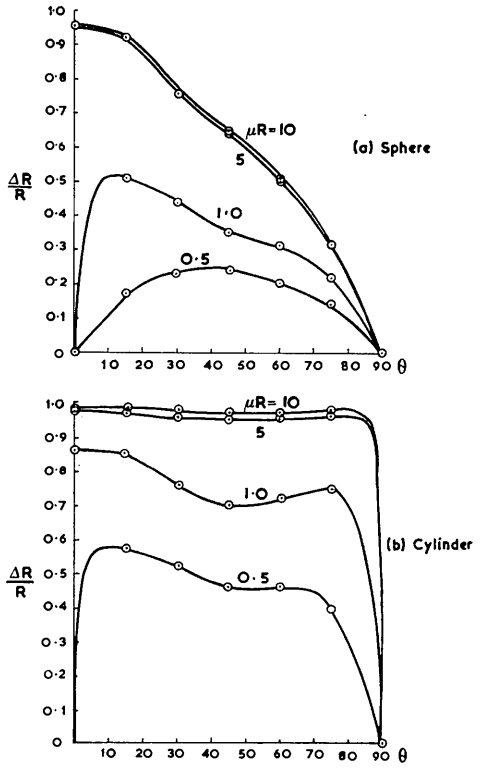

Fig. 9. The variation of line displacement with Bragg angle.

This paper is published by permission of the Central Electricity Generating Board.

APPENDIX

Calculation of the intensity of line profiles

Consider the shaded regions of a spherical and cylindrical specimen as shown in Fig. 4. The intensity of the reflected beam emerging from the region of volume ΔV_{sph} of the sphere is given by

$$I = kI_0 A \Delta V_{\text{sph}} \tag{A.1}$$

where k is a physical constant, I_0 is the intensity of the incident X-rays and A is the X-ray transmission factor of the region. Equation (2.19) gives the relevant expression for the product $A\Delta V_{\text{sph}}$

$$A\Delta V_{\text{sph}} = \frac{R^2}{4} \sin^2 \alpha/2 \int_0^{2\pi} \sin \beta/2 \times \int_0^c \exp\left[-\mu(p+c-x)\right] \mathrm{d}x \mathrm{d}\beta \mathrm{d}\alpha \,. \tag{A.2}$$

If we consider the volume ΔV_{sph} to be infinitely narrow we can divide ΔV_{sph} by its thickness

$$R \sin \frac{\alpha}{2} \frac{\mathrm{d}\alpha}{2}$$

to obtain

$$A\Delta V_{\text{sph}} = \frac{R}{2} \sin \frac{\alpha}{2} \int_0^{2\pi} \sin \frac{\beta}{2} \times \int_0^c \exp\left[-\mu(p+c-x)\right] \mathrm{d}x \mathrm{d}\beta \,. \tag{A.3}$$

Thus, for a sphere the intensity of any line element of the profile obeys the proportionality

$$I \propto \sin \frac{\alpha}{2} \int_0^{2\pi} \sin \frac{\beta}{2} \int_0^c \exp\left[-\mu(p+c-x)\right] \mathrm{d}x \mathrm{d}\beta \,. \tag{A.4}$$

Equation (2.22) gives for a cylinder of height, h,

$$A\Delta V_{\text{cyl}} = \frac{R}{2} h \sin \frac{\alpha}{2} \int_0^c \exp\left[-\mu(p+c-x)\right] \mathrm{d}x \mathrm{d}\alpha \,. \tag{A.5}$$

Again if the shaded region of volume ΔV_{cyl} is assumed to be infinitely narrow (A.5) reduces to

$$A\Delta V_{\text{cyl}} = h \int_0^c \exp\left[-\mu(p+c-x)\right] \mathrm{d}x \,. \tag{A.6}$$

Hence for a cylinder the intensity of any line element of the profile obeys the proportionality

$$I \propto \int_0^c \exp\left[-\mu(p+c-x)\right]\mathrm{d}x\,. \qquad \text{(A.7)}$$

References

BOND, W. L. (1959). *Acta Cryst.* **12**, 375–381.

CLAASEN, A. (1930). *Phil. Mag.* **9**, 57–65.

DWIGGINS, C. W. JR (1974). *Acta Cryst.* A**31**, 146–148.

DWIGGINS, C. W. JR (1975). *Acta Cryst.* A**31**, 395–396.

EVANS, H. T. & EKSTEIN, M. G. (1952). *Acta Cryst.* **5**, 540–542.

International Tables for X-ray Crystallography (1959). Vol. II, pp. 291–305. Birmingham: Kynoch Press.

TAYLOR, A. & SINCLAIR, H. (1945). *Proc. Phys. Soc.* **57**, 108–125.

WEBER, K. (1967). *Acta Cryst.* **23**, 720–725.

WEBER, K. (1969). *Acta Cryst.* B**25**, 1174–1178.

Acta Cryst. (1976). A**32**, 648

Transmitted-Beam Absorption Pattern from a Turbostratic Structure: Pyrolytic Graphite

BY L. D. CALVERT*

Division of Chemistry, National Research Council of Canada, Ottawa, Canada, K1A OR9

AND R. C. G. KILLEAN† AND A. MCL. MATHIESON

Division of Chemical Physics, CSIRO, P.O. Box 160, *Clayton, Victoria, Australia* 3168

(*Received* 16 *January* 1976; *accepted* 29 *January* 1976)

By the use of Cu $K\alpha_1$ plane-polarized X-rays, the intensity of the beam transmitted through a plate of highly oriented pyrolytic graphite is measured as the plate is tilted (ω) relative to the beam. The resultant transmitted-beam absorption pattern(TBAP), expressed as effective attenuation coefficient, μ', *versus* ω, is interpreted in relation to the turbostratic structure of pyrolytic graphite. The TBAP, μ' *versus* ω, is complementary to the diffraction pattern, presented as log I *versus* 2θ. Potential uses of the TBAP are discussed.

Introduction

In studies of the X-ray polarization ratio for 000*l* reflexions from highly oriented pyrolytic graphite (HOPG) (Calvert, Killean & Mathieson, 1974*a*), the intensity of the transmitted X-ray beam was measured. From a selected range of these measurements, the attenuation coefficient, μ, of carbon for Cu $K\alpha_1$ was deduced (Calvert, Killean & Mathieson, 1975). The transmitted-beam measurements, extended to cover the angular range of the specimen, $\omega = 10$ to 95° ($\omega = 90°$ corresponded to the beam normal to the plane of the specimen), and converted to the effective attenuation coefficient, μ', illustrate the scattering process which occurs with a turbostratic specimen. The derived transmitted-beam absorption pattern, μ' *versus* ω, can be considered as complementary to the diffraction pattern, given as log I *versus* 2θ.

Attention is drawn to the implications of these observations for the determination of accurate attenuation coefficients and accurate absolute intensities.

Experimental

The specimen used was a plate of HOPG (Union Carbide Co., grade ZYA), dimensions approximately $1 \times \frac{1}{2} \times \frac{1}{20}''$ ($2{\cdot}5 \times 1{\cdot}25 \times 0{\cdot}11$ cm) with a nominal crystalline angular spread of $\frac{1}{2}°$ (Moore, 1973). The plate could be tilted (Mathieson, 1968) with respect to the incident beam of plane-polarized Cu $K\alpha_1$ X-rays (Calvert, Killean & Mathieson, 1974*b*) of circular cross section and having a divergence of $\pm 7'$ of arc (aperture near effective source, 1·4 mm, aperture near specimen, 1·66 mm, separation 398 mm) and intensity 16000 counts/s (c/s). The dead time of the counting system ($2{\cdot}54 \times 10^{-6}$ s) was measured by the method of Chipman (1969); the background count rate was 0·15 c/s; counting times were chosen to give precisions ranging between 0·15 and 0·5%. The angular range studied was from $\omega = 95$ to 10°. This gave a range of count rates from 6000 c/s to 20 c/s over a sixfold increase of path length through the specimen; the mean thickness of the specimen, 0·1091 cm, was measured by a specially constructed Sheffield air gauge and also with the aid of a sensitive micrometer (*vide* Calvert, Killean & Mathieson, 1975).

The incident X-ray beam was plane polarized in a vertical plane and the specimen tilt axis was also

---

* N.R.C. No. 15309.

† On leave from School of Physical Sciences, University of St. Andrews, North Haugh, St. Andrews, Scotland KY16 9SS.